Int. J. Electrochem. Sci., 12 **(2017)** 10863 – 10881, doi: 10.20964/2017.11.34

International Journal of
ELECTROCHEMICAL
SCIENCE
www.electrochemsci.org

Influence of Sodium Tungstate and Sealing Treatment on Corrosion Resistance of Coatings Formed on AZ31 Magnesium Alloy by Plasma Electrolytic Oxidation

Wenbin Tu, Yulin Cheng, Tingyan Zhan, Junxiang Han, Yingliang Cheng *

College of Materials Science and Engineering, Hunan University, Changsha, 410082, China
*E-mail: chengyingliang@hnu.edu.cn, deepblacksea@163.com

Received: 2 August 2017 / *Accepted:* 9 September 2017 / *Published:* 12 October 2017

W-containing ceramic coatings were fabricated on AZ31 magnesium alloy by plasma electrolytic oxidation (PEO) in an aluminate-based electrolyte with the addition of sodium tungstate ($Na_2WO_4 \cdot 2H_2O$). The addition of $Na_2WO_4 \cdot 2H_2O$ not only increased the growth rate and surface roughness of the coatings but also improved the corrosion resistance of the PEO coating. The relationship between the corrosion resistance of the PEO coating and the concentration of $Na_2WO_4 \cdot 2H_2O$ was studied, and the coating obtained in 10 g l^{-1} $Na_2WO_4 \cdot 2H_2O$ showed the best corrosion resistance. Ce-based sealing followed by $Al(H_2PO_4)_3$ sealing treatment was further carried out to improve the corrosion resistance of the coatings. It was found that the number and size of pores and micro-cracks decreased after sealing. Potentiodynamic polarization tests and electrochemical impedance spectroscopy (EIS) measurements indicated that the corrosion resistance of the PEO coatings was effectively improved by the two-step sealing method.

Keywords: Plasma electrolytic oxidation, Magnesium alloy, Tungstate, sealing, corrosion resistance.

1. INTRODUCTION

Due to their excellent properties such as good castability, low density, high strength-to-weight ratio, good electromagnetic shielding and damping characteristics, a great number of studies have been done on magnesium and its alloys [1-3]. In spite of their excellent properties, the poor corrosion resistance of magnesium and its alloys is one of the main obstacles that limits its extensive application, especially in aggressive environments. Therefore, attempts are needed to improve the corrosion resistance of magnesium and its alloys [4].

Plasma electrolytic oxidation (PEO) is an useful method to improve the corrosion and tribological properties of valve metals such as aluminum and magnesium, because after PEO treatment, thick oxide layer is formed on the surface of metal, which can slow down the corrosion rate and protect the substrate from being worn quickly [1, 5]. The microstructure and properties of PEO coating are determined by many factors, such as the kind of substrate, electric regimes, type and concentration of electrolyte [6-9], among which the last one plays an important role.

There is much recent interest in using valve metals for PEO treatment in electrolytes with sodium tungstate to synthesize WO_3 containing ceramic coatings with good photocatalytic activity, semiconductive properties and better wear and corrosion resistance [10]10. Tseng [11] and Li [12] studied the properties of PEO coatings before and after the addition of sodium tungstate to electrolyte, but they did not investigate the influence of sodium tungstate concentration on the microstructure and corrosion resistance of the PEO coatings. Zheng [13]13 deposited alumina coating in a H_3BO_3–KOH electrolyte solution with the addition of Na_2WO_4; they found that increasing the Na_2WO_4 concentration in the electrolyte led to a reduced coating thickness, which seems to contradict the usual understanding of the role Na_2WO_4 plays in the PEO process [14].

In our previous work [14], black W-containing coatings on Mg alloy were successfully fabricated by PEO in aluminate-tungstate electrolyte. The cell potential-time responses, coating morphology, and phase composition before and after the addition of Na_2WO_4 was investigated. Based on the results of sequential anodizing, a mechanism for the development of the coating at later stage of PEO process was put forward. However, the relationship between Na_2WO_4 concentration and corrosion resistance of PEO coatings was not discussed in that report.

In general, the PEO coating on magnesium is divided into three layers: a porous outer layer with low hardness, a more compact and denser intermediate layer beneath the outer layer and a thin barrier layer in contact with the substrate [15, 16]. Pores within the outer layer of coating make it easy for corrosive media to penetrate into coating, which is not good for the long-term service of the metal. Concerning the structural properties of the PEO coating, it might be a feasible approach to reduce their porosity by blocking the pores in the coatings via post-treatment sealing techniques. To date, a lot of different post-treatment methods for PEO coatings such as alkaline [17], sol-gel sealing [18, 19], hydrothermal sealing [20]20 as well as rare earth-based sealing treatments [21]21 have been carried out by researchers. Among these methods, the cerium-based sealing treatment is considered an effective and promising approach for PEO coatings on magnesium as a result of comprehensive considerations about costs, efficiency and environmental compatibility [22, 23]. Despite cerium-based sealing having been reported to be an effective method to increase the corrosion resistance of valve metals, most cerium-based sealing treatments are only a one-step treatment. Thus, whether post-treatment after cerium-based sealing can further influence the corrosion resistance of PEO coating is still not clear.

Phosphate ions can react with many positively charged metal ions to form insoluble phosphorous compounds and deposits on a metal surface, which are frequently applied in coating sealing treatments to increase the corrosion resistance of the substrate material [24-26]. Sealing with aluminium phosphate originates from the field of refractories and their binders, and it has been widely used in many organic coatings [27, 28]. However, the application of sealing PEO coatings with

aluminium phosphate has seldom been reported. Phuong [29] conducted cerium and phosphate-based sealing treatments on magnesium, and the corrosion resistance of the coating was reported to be improved, but the corrosion resistance was only measured by polarization tests. No electrochemical impedance spectroscopy tests were carried out, and the corrosion mechanisms were not investigated. In this paper, the influence of sodium tungstate concentration on the coating microstructure and corrosion resistance of the PEO coatings is investigated. In addition, cerium-based sealing treatment followed by $Al(H_2PO_4)_3$ sealing is carried out for the fabricated PEO coatings; the microstructure differences and corrosion behaviour of the coatings before and after sealing are compared; and the corrosion mechanisms of the coatings are also explored in the present study.

2. EXPERIMENTAL

2.1 Materials and PEO treatment

A rolled AZ31 magnesium alloy plate was chosen as the substrate for the PEO treatment. An aluminate-based alkaline solution (10 g l^{-1} $NaAlO_2$, 3 g $l^{-1}$$C_6H_8O_7 \cdot H_2O$, 2 g l^{-1}KOH) with addition of 0, 10 and 20 g l^{-1} $Na_2WO_4 \cdot 2H_2O$ was used as the PEO electrolyte. A pulsed bipolar constant current mode was employed for the PEO treatment, with average positive and negative current densities of ~ 0.22 and ~0.09 Acm^{-2}, respectively. The duty cycle was kept at 20%. The frequencies of the PEO treatment were first set at 1000 Hz and then coatings formed with 100 Hz were also investigated. The details of experiments are largely the same as those in literature [14].

2.2 Sealing treatment

Two different sealing solutions were prepared for the PEO coatings formed with a current frequency of 100 Hz. The cerium solution was composed of 10 g l^{-1} $Ce(NO_3)_3 \cdot 6H_2O$, 10 g l^{-1} H_2O_2 and 2 g l^{-1} H_3BO_3. The phosphate solution was composed of 50 g l^{-1} $Al(H_2PO_4)_3$. PEO coated AZ31 magnesium was first immersed in the cerium solution for 3 h at 40℃. After that, the phosphate sealant was spread onto the coatings at room temperature and stood for 12 h. Then, the samples were heat-treated at 250°C for 40 min.

2.3 Coating characterization

The thickness of the coatings was measured at 12 different spots of the coating surface by an eddy current thickness gauge (TT260, Time Group, Beijing), and then an average value was calculated. The same method was applied to determine the surface roughness (Ra and Rz) of coatings by a stylus profilometer (Mitutoyo SJ-210). The surface and cross-sectional morphologies of the PEO coatings were examined by scanning electron microscopy (SEM, QUANTA 250, FEI, USA). For cross-sectional observation, the specimens were ground with successive grades of SiC paper, followed

by diamond finishing to 1 μm. The phase compositions of the coatings were determined with a Rigaku D/MAX 2500 X-ray diffractometer (Cu–Kα radiation).

2.4 Electrochemical measurement

The electrochemical behaviours of the sealed and unsealed samples were determined by recording the potentiodynamic polarization curves using a CHI660C electrochemical workstation. A naturally-aerated 3.5 wt.% NaCl solution was selected for the corrosion tests in a conventional three-electrode test cell, with a platinum counter electrode, a saturated calomel reference electrode and the specimen as the working electrode. The open circuit potential (OCP) for the specimens was recorded for a duration of 1800 s, then potentiodynamic polarization curve was performed at a scan rate of 0.5 mV s^{-1} from ~ -0.5 V to 1.5 V with respect to the OCP. After immersion for 1 h in 3.5 wt.% NaCl solution, electrochemical impedance spectroscopy (EIS) measurements were carried out with frequency ranging from 10 mHz to 10^5 Hz, using a sinusoidal potential perturbation of ±10 mV, with at least 5 points per logarithmic unit. The obtained figures were then fitted by ZsimpWin software.

3. RESULTS AND DISCUSSION

3.1 Coating thickness and roughness

The coating growth kinetics for different concentrations of Na_2WO_4 is shown in Fig. 1. It can be noted that addition of Na_2WO_4 to the electrolyte increased the growth rate of the PEO coatings. The average growth rate for 0, 10 and 20 g l^{-1} Na_2WO_4-containing electrolyte is ~ 4.8, 6.8 and 8.2 μm per minute, respectively. Due to the higher growth rate in electrolyte with 20 g l^{-1} Na_2WO_4, for the preparation of samples for corrosion tests, the duration of PEO treatment lasted for only 480 s for the electrolyte with 20 g l^{-1} Na_2WO_4, and the coatings formed in the other two electrolytes were treated for 600 s. Thus, similar coating thicknesses were maintained for different coatings, which makes the comparison of corrosion resistance between coatings more reliable.

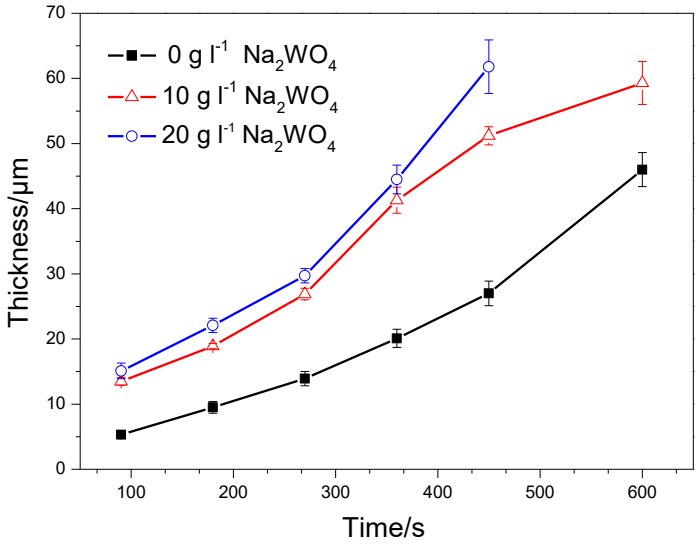

Figure 1. Dependence of coating thickness on time of PEO for coatings formed under different concentrations of $Na_2WO_4 \cdot 2H_2O$. Error bars represent the standard deviations.

Fig. 2 depicts the thickness and roughness of coatings with different concentrations of Na_2WO_4. It is noted that the thickness of coatings increased as more Na_2WO_4 was added to the electrolyte. After 600 s PEO treatment, the average thickness of the PEO coating is 46 ± 1.2 μm in Na_2WO_4-free electrolyte; while it is 59.3 ± 3.3 μm for PEO coating fabricated in aluminate electrolyte with the addition of 10 g l^{-1} Na_2WO_4 to the same aluminate-based electrolyte. The average thickness of the coatings is 64.7 ± 4.4 μm for electrolyte with 20 g l^{-1} Na_2WO_4 after treated for 480 s. The surface roughness of the coating is assessed by parameters Ra, which is the arithmetical mean deviation of the profile, and Rz, which shows the average peak to valley height. According to Fig. 2, it is obvious that the two parameters increase with the increase of electrolyte concentration, with Ra varying from 3.51 to 8.84 μm and Rz varying from 23.41 to 46.62 μm. This means electrolyte concentration not only affects the growth rate of the PEO coating but also influences the surface features of the coating.

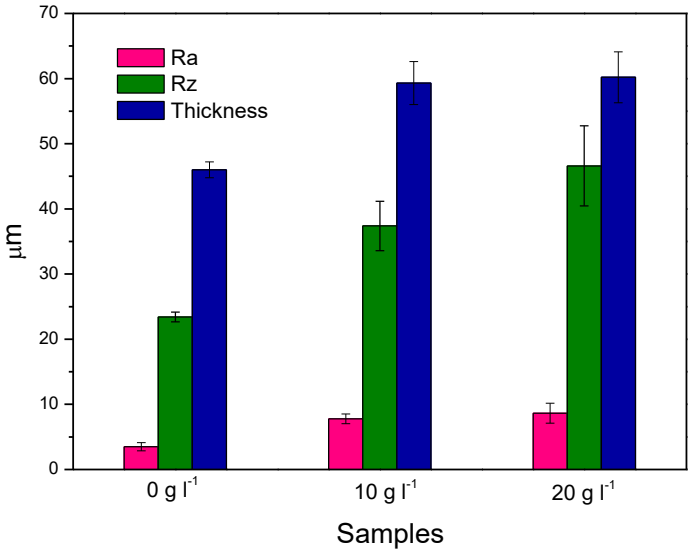

Figure 2. Thickness and surface roughness parameters of Ra and Rz for the coatings formed for 600 s in electrolytes with the addition of 0 and 10 g l^{-1} $Na_2WO_4 \cdot 2H_2O$ and the coating formed for 480 s in 20 g l^{-1} $Na_2WO_4 \cdot 2H_2O$

3.2 Phase composition of the coatings before and after sealing

The phase compositions of the coatings before and after sealing are compared in Fig. 3. The coatings were formed by PEO for 600 s with the addition of 10 g l^{-1} Na_2WO_4. As shown in Fig. 3(a), the original coating is mainly composed of MgO and $MgAl_2O_4$. Protruding Mg peaks were detected, and this can be attributed to the porous nature of the coating. WO_3 and $W_{18}O_{49}$ peaks were also detected. The phase composition of the sealed sample is depicted by Fig. 3(b), which is quite different from the unsealed coating. A prominent peak of $AlPO_4$ was detected, and peaks of $Al(PO_3)_3$, $Al(H_2PO_4)_3$ and a weak peak of $AlH_2P_3O_{10}$ were observed in the pattern. The XRD results presented here signify that $Al(H_2PO_4)_3$ was partly decomposed during heat treatment. During heat treatment to

250℃, a series of chemical reactions occurred for the hydrated aluminum dihydrogen phosphate ($(Al(H_2PO_4)_3 \bullet xH_2O$).

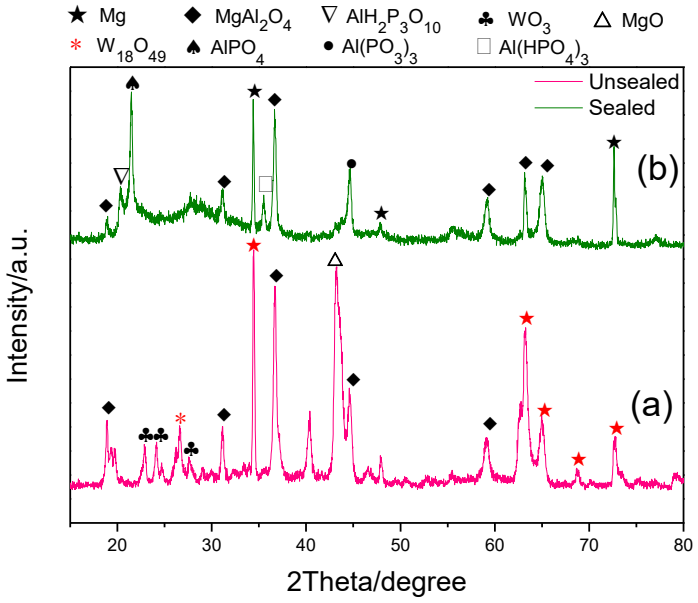

Figure 3. XRD patterns of the unsealed (a) and sealed (b) PEO coatings formed in the aluminate-based electrolytes with addition of 10 g l^{-1} $Na_2WO_4 \cdot 2H_2O$.

At around 105℃, $Al(H_2PO_4)_3 \bullet xH_2O$ dehydrated to $AlH_2(PO_4)_2 \bullet H_2O$, and when the temperature was further increased to 200℃, $Al(H_2PO_4)_3$, which is a very effective binding phase, was generated; at approximately 220℃, $Al(H_2PO_4)_3$ was converted to $AlH_2P_3O_{10}$ (Aluminium Tripolyphosphate, ATP) accompanied by the formation of $AlPO_4$ [30]. Ce-containing oxide was not observed in the pattern. This might because of either the atom ratio of Ce in the sealed coating is too low to be detected or the first step of treatment is not sufficient for homogeneous deposition to occur.

3.3 Surface morphologies and potentiodynamic curves of the coatings

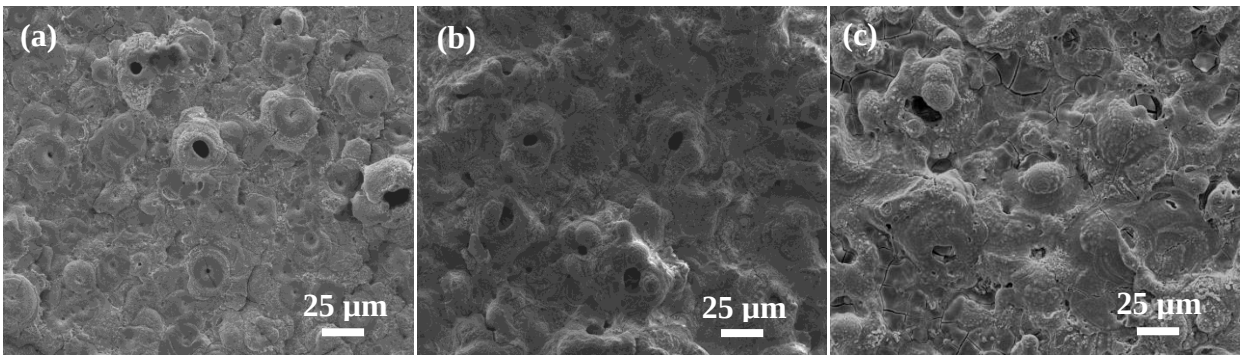

Figure 4. Surface morphologies of the coatings formed for 600 or 480 s in the aluminate-based electrolyte with the addition of different $Na_2WO_4 \cdot 2H_2O$ concentrations. (a) 0 g l^{-1} $Na_2WO_4 \cdot 2H_2O$, 600 s; (b) 10 g l^{-1} $Na_2WO_4 \cdot 2H_2O$, 600 s; (c) 20 g l^{-1} $Na_2WO_4 \cdot 2H_2O$, 480 s.

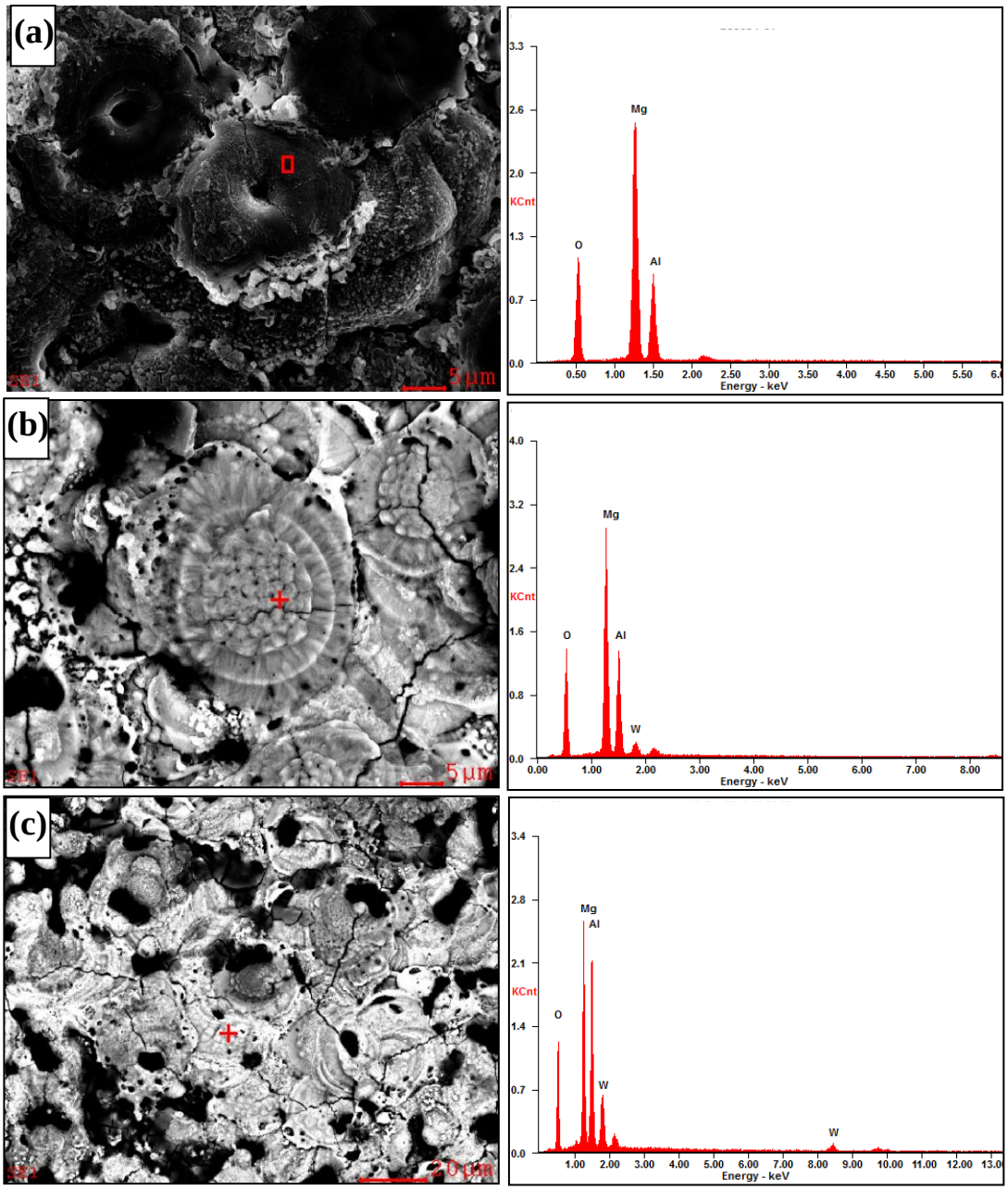

Figure 5. Magnified surface morphologies of the coatings formed for 600 or 480 s in the aluminate based electrolyte with the addition of different $Na_2WO_4 \cdot 2H_2O$ concentrations and the EDS spectra for the marked area. (a) 0 g l^{-1} $Na_2WO_4 \cdot 2H_2O$, 600 s; (b) 10 g l^{-1} $Na_2WO_4 \cdot 2H_2O$, 600 s; (c) 20 g l^{-1} $Na_2WO_4 \cdot 2H_2O$, 480 s.

The surface morphologies of the coatings were examined by scanning electron microscopy (SEM), and the results are presented in Fig. 4. As shown in the figure, pancake structure with central

pores is the dominant feature of the coatings formed in the Na_2WO_4-free electrolyte. However, the pancakes are not so apparent for the coatings fabricated in Na_2WO_4-containing electrolyte and the surfaces are rougher. In addition, the number and size of micro pores increased and a number of micro-cracks were observed on the coating surface obtained in aluminate electrolyte with 20 g l^{-1} Na_2WO_4, as seen in Fig.4(c). Aluminate electrolytes were also used by Hussein [31, 32] in the PEO treatment for magnesium alloy, the surface morphologies of coatings in those literatures were also reported to be characterized by a number of pancake structures. However, when aluminate electrolyte was replaced by silicate- or phosphate-based electrolytes, no pancake structure was reported to in literature [33] and [34]. Therefore, the appearance of pancake structure might have relationship with the incorporation of Al species in the coating. According to results of XRD examination, one of the main phases in the coating is $MgAl_2O_4$, which is an electrical dielectric with a band gap of at around 7.8 eV [35]. Report [7] pointed out that PEO coating structure has a close relationship with the electronic property of the PEO coatings; i.e., pancake structure is usually formed when the proportion of insulating dielectric oxide is high in PEO coating. Thus, the appearance of pancake structure is attributed to $MgAl_2O_4$ in the coating.

For a better understanding of the relationship between the microstructure and electrolyte concentration, the magnified surface morphologies of samples were examined and the results are shown in Fig. 5. Energy dispersive spectrometer (EDS) analyses were also carried out for the marked areas in Fig. 5 and the results of the element proportions are summarized in Table 1. According to Table 1, the atom ratio of Al species increased along with increase of $Na_2WO_4{\cdot}2H_2O$ concentration, but changes of weight ratio for Al seems not obvious. This is because element W, relative atomic mass of which is much greater than that of Al, took part in the coating formation. XRD test results signified that Al exists in the coating in the form of $MgAl_2O_4$. That is to say, apart from the increase in the proportion of tungstate oxides, the content of $MgAl_2O_4$ also increased after adding more $Na_2WO_4{\cdot}2H_2O$ to the electrolyte. Lu [36] and Sandhyarani [37] noted out that increasing the electrolyte concentration can raise the electrical conductivity of the electrolyte, thus activating plasma reaction of the PEO process; in the present study, the PEO process became more intensive and loud noise could be heard after adding more $Na_2WO_4{\cdot}2H_2O$ to the electrolyte, which means more ions participated in the coating formation. Therefore, the atom ratio of both Al and W increased in the coating, which may have contributed to the changes in coating structure.

Table 1. EDS analysis of the positions as indicated in Fig. 5(a),(b),(c)

Sample	Element composition in Wt% and At% (the values in brackets), respectively.			
	O	Mg	Al	W
a	32.13 (42.73)	43.24 (37.84)	24.63 (19.42)	-
b	29.55 (43.88)	33.93 (33.14)	24.30 (21.39)	12.23 (01.58)
c	24.72 (41.92)	23.89 (26.64)	27.84 (27.97)	23.54 (03.47)

It was known in previous study that the anions from the electrolyte can contribute significantly to the coating growth [38]. That is why coatings formed in electrolytes with the addition of high concentrations of tungstate show higher growth rate. It was also noted that plasma discharges are stronger during the PEO in electrolytes with more tungstate addition. Thus, it is expected that the amount of the molten oxide will also increase correspondingly, resulting in an increase in the protuberances and hence higher surface roughness.

On the other hand, based on the coating growth mechanism proposed in literature [14], the micro-discharge current density within discharge channels was estimated to be about 10^4 Acm^{-2}, when the number of sparks decreases, this value is even larger, leading to a higher temperature at a fixed spot, so more magnesium substrate was molten and participated in the coating formation process. The molten hot mixture of substrate and oxides was transferred to the coating surface under the force of gas flow, leading to accumulation of materials and a more rough surface was developed. Formation of occasional micro-cracks can be attributed to the thermal stress due to the rapid solidification of the hot molten oxide in the relatively cool electrolyte [39].

The corrosion behaviors of the coatings prepared in the aluminate-based electrolyte with the addition of 0,10 and 20 g l^{-1} $Na_2WO_4 \cdot 2H_2O$ and also the uncoated substrate have been evaluated by potentiodynamic polarization tests in 3.5 wt% NaCl solution.

The corresponding electrochemical data, namely anodic and cathodic Tafel slopes (b_a and b_c), E_{corr} and i_{corr} derived from the polarization curves, the polarization resistance (Rp) values were determined using Stern–Geary equation [6, 39]:

$$R_p = \frac{b_a \, b_c}{2.303 i_{corr}(b_a + b_c)}$$

Fig.6 displays the results of the polarization curves for the uncoated and coated AZ31 magnesium alloys. All the above corrosion parameters obtained from Tafel extrapolation method for the samples are listed in Table 2.

In a typical polarization curve, a higher corrosion potential or a lower free-corrosion current density is usually related to a better corrosion resistance or a lower rate of corrosion [40]. In the present study, all of the PEO-treated samples showed higher corrosion potentials than the untreated magnesium alloy did. Generally, the anodic polarization curve is related to the electrochemical dissolution of metal substrate, namely, magnesium in the present study, and the cathodic polarization curve is attributed to cathodic hydrogen evolution during water reduction [41]. It can be found in table 2 that anodic Tafel slopes b_a for the PEO coated specimen are smaller than that of the magnesium substrate, furthermore, PEO coatings shown much higher polarization resistance compared with bare magnesium alloy, indicating the oxide films fabricated through PEO treatment can slow down the anodic potential reaction rate. For the PEO coatings, the addition of tungstate to the PEO electrolyte was found to result in lower free-corrosion current densities (j_{corr}) compared to that of the coating formed in the aluminate based electrolyte. The lowest corrosion density was found with the coating formed with 10 g l^{-1} $Na_2WO_4 \cdot 2H_2O$, being 8.22×10^{-7} Acm^{-2}, which is significantly lower than that of the substrate (2.45×10^{-4} Acm^{-2}). As for the polarization resistance of the PEO coated samples, the coating fabricated in aluminate electrolyte with 10 g l^{-1} $Na_2WO_4 \cdot 2H_2O$ has the biggest value, being 4.56×10^7 $\Omega\,cm^{-2}$, while it's 4.57×10^{-6} Acm^{-2} and 8.22×10^6 $\Omega\,cm^{-2}$ for the coating fabricated in W-free

aluminate-based electrolyte. The above results indicates that adding $Na_2WO_4 \cdot 2H_2O$ to the electrolyte can somehow improve the corrosion resistance of the PEO coatings. Tseng et al. [11] investigated the influence of sodium tungstate on corrosion resistance of PEO coatings formed on aluminium alloy, they pointed out that corrosion resistance of coatings were improved along with increment in concentration of sodium tungstate, which is in accord with the results of present study. However, when concentration of $Na_2WO_4 \cdot 2H_2O$ was further increased to 20 g l^{-1}, the current density and polarization resistance were found to be slightly reduced, but were still higher than those of coatings obtained in $Na_2WO_4 \cdot 2H_2O$-free electrolyte, the decrease in current density and polarization resistance is mainly attributed to more pores and cracks within the coating, making it easier for transportation of corrosive media.

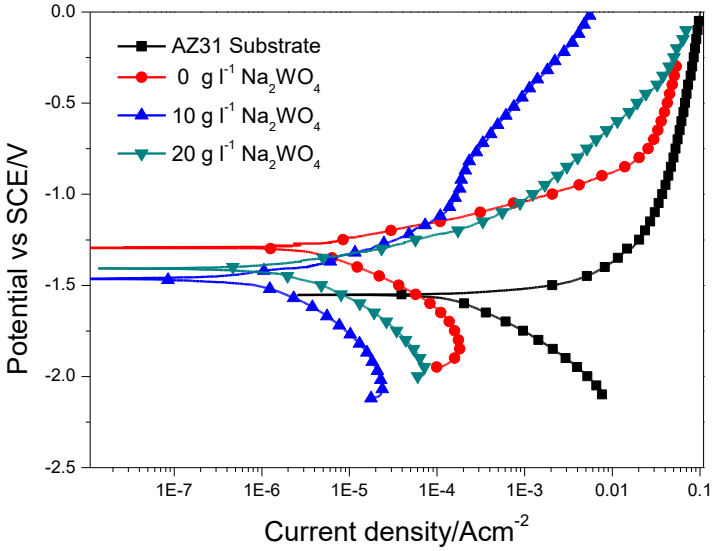

Figure 6. Potentiodynamic polarization curves for the uncoated and PEO-coated AZ31 magnesium alloys. The coatings are formed in aluminate-based electrolyte with different addition $Na_2WO_4 \cdot 2H_2O$ concentrations.

Table 2. Corrosion parameters for the uncoated alloy and the alloy coated in the aluminate-based electrolyte with the addition of 0-20 g l^{-1} $Na_2WO_4 \cdot 2H_2O$ (data obtained from the potentiodynamic polarization curves in Fig.6).

Samples	b_a(mV/decade)	b_c(mV/decade)	E_{corr}(V)	j_{corr}(A·cm^{-2})	Rp(Ω·cm^{-2})
Substrate	168.6	223.4	-1.554	2.45×10^{-4}	1.703×10^{5}
0 g l^{-1}	133.1	243.7	-1.293	4.57×10^{-6}	8.22×10^{6}
10 g l^{-1}	113.5	362.2	-1.467	8.22×10^{-7}	4.56×10^{7}
20 g l^{-1}	150.5	257.6	-1.407	1.97×10^{-6}	2.09×10^{7}

3.4 Microstructure of the unsealed and sealed coatings fabricated at a frequency of 100 Hz

The above studies are based on the coatings formed at a frequency of 1000 Hz, which was also the frequency used in our previous study [14]. The polarization curves show that adding

$Na_2WO_4 \cdot 2H_2O$ to electrolyte can improve the corrosion resistance of PEO coating. However, too much $Na_2WO_4 \cdot 2H_2O$ in the electrolyte leads to more intensive discharges, generating micro defects in the coating, which is not good for corrosion protection. From this study, 10 g l^{-1} $Na_2WO_4 \cdot 2H_2O$ yields the best corrosion protection. In this section, coatings formed under a lower frequency, 100 Hz, is also investigated. It was noted that when the frequency changed from 1000 to 100 Hz, milder plasma discharges were observed; the sound emission during PEO discharge was softer and the number of moving sparks increased. Based on the relationship between discharge intensity and microstructure, it might be presumed that coating fabricated under 100 Hz may have a more compact layer structure, thus providing a better protection to the alloy. To verify this hypothesis, AZ31 specimens were treated for 600s in aluminate electrolyte with 10 g l^{-1} $Na_2WO_4 \cdot 2H_2O$ under a frequency of 100 Hz, and the microstructure of the obtained PEO coating was examined by SEM and the results are depicted in Fig.7. Pancake structure is still the dominant feature for surface morphology of the coating, as illustrated in Fig.7 (a), few micro-pores randomly distributed on the surface. The whole coating looks smoother than the coating formed in the same electrolyte under 1000 Hz. Ra and Rz were measured to be 4.87 and 29.60 μm respectively, smaller than that of its counterpart under 1000 Hz. Cross-sectional morphology of the coating is shown in Fig.7 (b), the coating exhibit a porous outer layer, a much thinner inner layer and a barrier layer at the interface of coating/substrate, similar to the PEO coating structure reported in [15] and [16]; average thickness of the coating was measured to be 52.9±3.1μm.

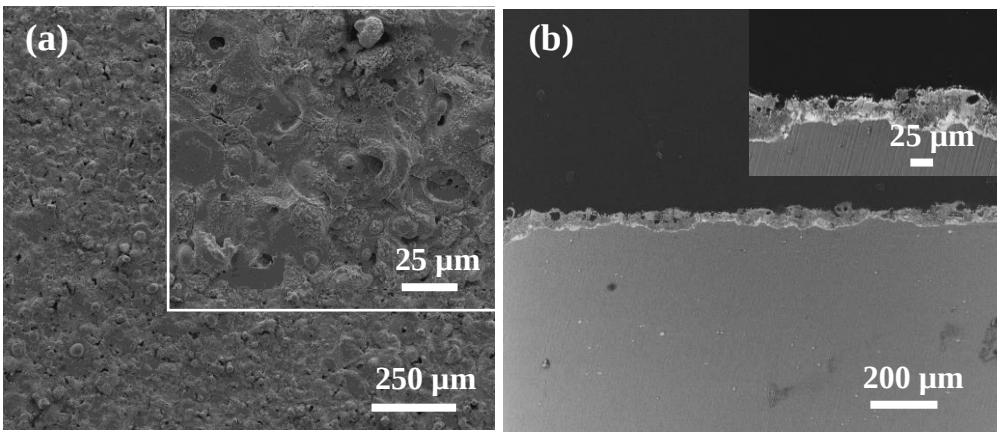

Figure 7. Surface and cross-sectional morphologies of the coating formed for 600 s in the aluminate-based electrolyte with addition 10 g l^{-1} $Na_2WO_4 \cdot 2H_2O$ under 100 Hz.

Despite a more compact coating was fabricated on AZ31 magnesium alloy, micro-pores still existed within the PEO coating, which might provide accesses for corrosive ions to migrate to the magnesium substrate. To slow down the corrosion rate of magnesium, sealing treatment was carried out for coating obtained under 100 Hz, the microstructure of the sealed coating is illustrated in Fig. 8. After sealing treatment, the pancake-like structure disappeared, and randomly distributed crater-like pores with a size ranging from 10-15 μm were replaced by a more uniform and homogeneous surface. Micro-pores still existed on the coating surface, but the size of which were ranging from 4-10μm,

much smaller than the PEO coated precursor. It can be noted that after sealing treatment, the number of pores within the coating was much smaller, as seen in Fig. 8(b) and (d).

The changes in coating structure are attributed to the chemical dissolution effect of acidic cerium solution by Mohedano [22]; when the main phase of the PEO coating, such as MgO and $MgAl_2O_4$ comes in contact with acidic cerium solution, converted products such as $Mg(OH)_2$ are formed, thus increasing the pH values [29]. On the other hand, H^+ produced by H_3BO_3 could partly dissolve oxides such as MgO in the coating, increasing the concentration of OH^- at a localized region. Furthermore, according to the work of Hu [42], as an oxidant, H_2O_2 can be decomposed and O_2 is released, after that, deoxidation of O_2 occur at cathodic sites, generating more OH^- at a fixed region, leading to increase of pH value of solution within pores in the coating, favoring the combination of Ce^{3+} and OH^- to form deposition in the pores. Therefore, the micro-pores within the coating were partly blocked with conversion products. In usual, the intermediate layer near substrate is thought to have close relationship with anti-corrosion ability of magnesium alloys [2]. Comparing Fig. 7(b) and Fig. 8(d), it can be seen that after sealing treatment, the white barrier inner layer between substrate and PEO coating remains. This means the ions in the sealing solution may only have reacted with oxide coating and failed to reach the substrate, which accords with the previous work of Mohedano [22].

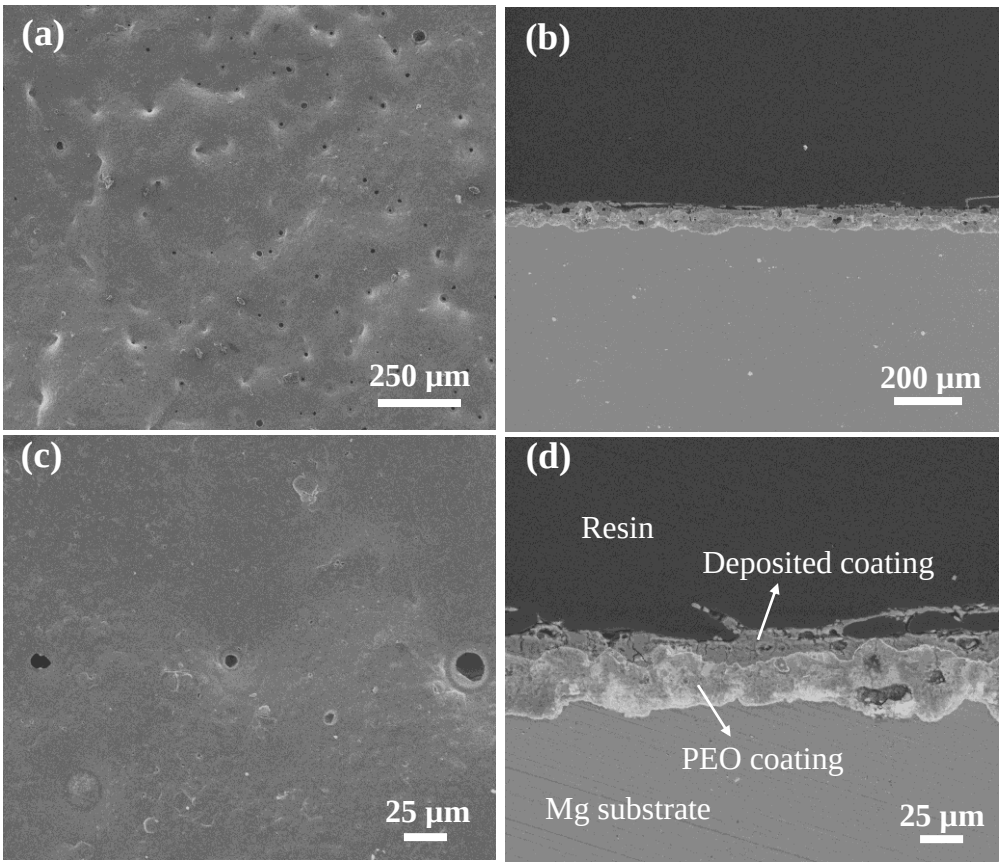

Figure 8. Surface and cross-sectional morphologies of the sealed coating formed for 600 s in the aluminate-based electrolyte with addition 10 g l^{-1} $Na_2WO_4 \cdot 2H_2O$ under a current frequency of 100 Hz. The cross sections are shown in backscattered electrons.

After being treated for 40 min under 250°C， the spread $Al(H_2PO_4)_3$ decomposed and solidified on the oxide coating surface, thus a thicker and uniform coating was formed. However, few micro-cracks were generated during solidification process. This might be ascribed to the thermal stress produced within the hybrid coating due to the difference in coefficient of thermal expansion between the original PEO coating and deposited coating.

3.5 Polarization curves of the unsealed and sealed samples

Potentiodynamic polarization curves of the unsealed and sealed samples fabricated under 100 Hz are shown in Fig. 9. The extracted E_{corr} are -1.306 and -1.289V (vs.SCE) and j_{corr} are 1.267×10^{-7} and 1.203×10^{-7} Acm^{-2} respectively. The anodic Tafel slopes b_a and cathodic slopes b_c are 104.7 and 374.4 mV/decade for the unsealed sample, while they are 97.6 and 391.3 mV/decade for the sealed sample. Comparing with the corrosion parameters of the unsealed coating obtained under 1000 Hz, as illustrated in Table 2, it can be noted that the E_{corr} shifted positively about 161mV and j_{corr} decreased after the current frequency changed from 1000 to 100 Hz, this is in accordance with the microstructure difference between samples formed under the two different frequency regime. After sealing treatment, E_{corr} slightly shifted positively and the j_{corr} was further decreased for specimen formed under 100 Hz, which means anticorrosion ability of the coating was improved. Slopes of cathodic polarization also decreased after sealing treatment, indicating the occurrence of pitting corrosion might be delayed, compared with unsealed coatings [39]. Phuong [29] conducted sealing treatment for PEO coating formed on magnesium alloy by immersing the coating in cerium and phosphate electrolyte, the free-corrosion current density was reported to be 1.1×10^{-7} Acm^{-2}, which is similar with the value in the presented study, however, corrosion mechanisms of the sealed coatings were not mentioned in that report.

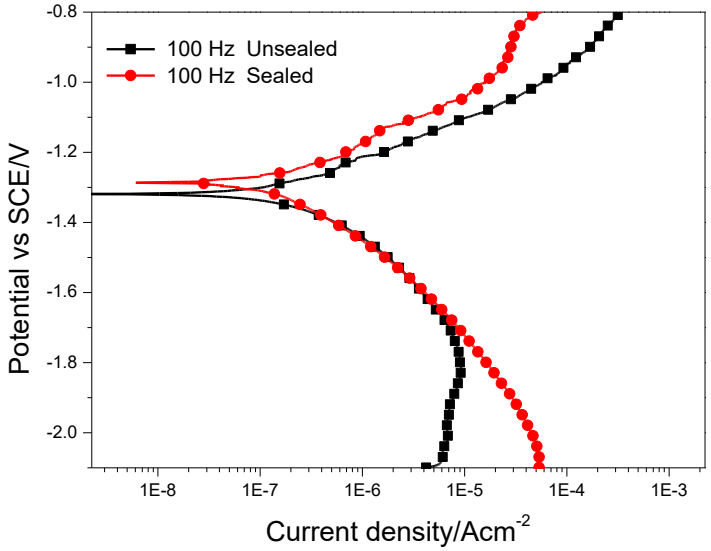

Figure 9. Potentiodynamic polarization curves for the unsealed and sealed PEO coatings formed for 600s in the aluminate-based electrolyte with the addition 10 g l^{-1} $Na_2WO_4{\cdot}2H_2O$ under a current frequency of 100 Hz.

For the purpose of a better understanding for the quantitative corrosion behavior of the hybrid coating system, EIS tests were carried out to investigate the corrosion process and the characterization

changes of the coatings before and after sealing treatment, which is significant to comprehend the corrosion mechanism of the coatings [43]. The EIS (Nyquist and Bode) plots, for bare Mg substrate, sealed and unsealed samples of 100 Hz, are compared in Fig. 10. Based on the proposed equivalent circuits, as illustrated in Fig.11, fitting was carried out and the fitted results are presented in Fig.10.

In the equivalent circuits, capacitors were replaced by constant phase element (CPE) as a result of the defective nature of the coatings and interface roughness [44]. The value of CPE were determined by $Z = 1/[C(j\omega)^n]$, in which C is the admittance constant, j represents the imaginary function ($j=\sqrt{-1}$), while ω represents radial frequency and n is the exponential factor($-1 \leq n \leq 1$). Chi-squared values for the fitting of bare Mg substrate, unsealed and sealed samples are 5.077×10^{-4}, 1.453×10^{-3} and 5.671×10^{-4}, respectively, which indicate that the experimental data is in good agreement with the proposed equivalent circuits. On the basis of the ascribed equivalent circuit, the fitted results are illustrated in Tables 3 and 4.

In the models, R_S is the resistance of the testing solution. In Fig.11 (a), R_1 is the resistance of oxide coating paralleled with a constant phase element (CPE1); R_L represents the charge-transfer resistance of pitting corrosion with the inductance L. In Fig. 11(b), R_1 corresponds to the resistive behavior of the combination of the deposited outer and intermediate porous outer layer of the PEO coating, which paralleled with CPE1. This combination response is proposed based on the division of the two layers of PEO coating: an outer layer, within which randomly distributed discharge channels and pores; a denser inner barrier layer [22]. R_2 represents the resistance of the barrier inner layer of the PEO coating paralleled with CPE2. R_3 is defined as the Faradaic charge transfer resistance in associated with electrochemical reactions took place at the interface of electrolyte/substrate, and CPE3 denotes the resistance of the double layer at the same region [45].

CPE is mainly related to the charge transfer process, while L and R_L are relevant to dissolution of Mg substrate and is indicative of pitting corrosion of the substrate [46]. It's evident that in the present study, the PEO coating has lower capacitance (CPE1-T) and higher resistance (R_1, R_L) compared with bare alloy, indicating the PEO coating can effectively protect the magnesium substrate from being quickly corroded, this conclusion complies with the result of polarization tests described before.

For the sealed coating, however, a totally different EIS behavior was observed. Comparing Nyquist plot of sealed and the enlarged unsealed sample, see in Fig. 10(a), it can be observed that there is no inductive loop for the sealed specimen. This result indicates that no pitting corrosion of the substrate may have occurred after immersion for 1 h in the corrosive electrolyte.

From another perspective, it's showed that the phase angles for the bare alloy and unsealed coating are less than 0°in low frequency range, see in Fig. 10(b), which signifies pitting corrosion took place at the surface; whereas, the phase angle for sealed sample is above 0°, indicating no pitting corrosion happened at low frequency range. This is in well agreement with the result derived from Nyquist plot.

Gowtham [47] pointed out that CPE-T value reflects the porosity level of the coating, lower CPE-T values are attributed to more compact oxide layers. By comparing the CPE1-T values before and after sealing, it can be observed that the sealed sample has a much lower value of CPE1-T,

signifying a more compact oxide layer and thereby better corrosion resistance of MAO coating [48]. This result is in accordance with the microstructure observed in Fig. 7 and Fig. 8.

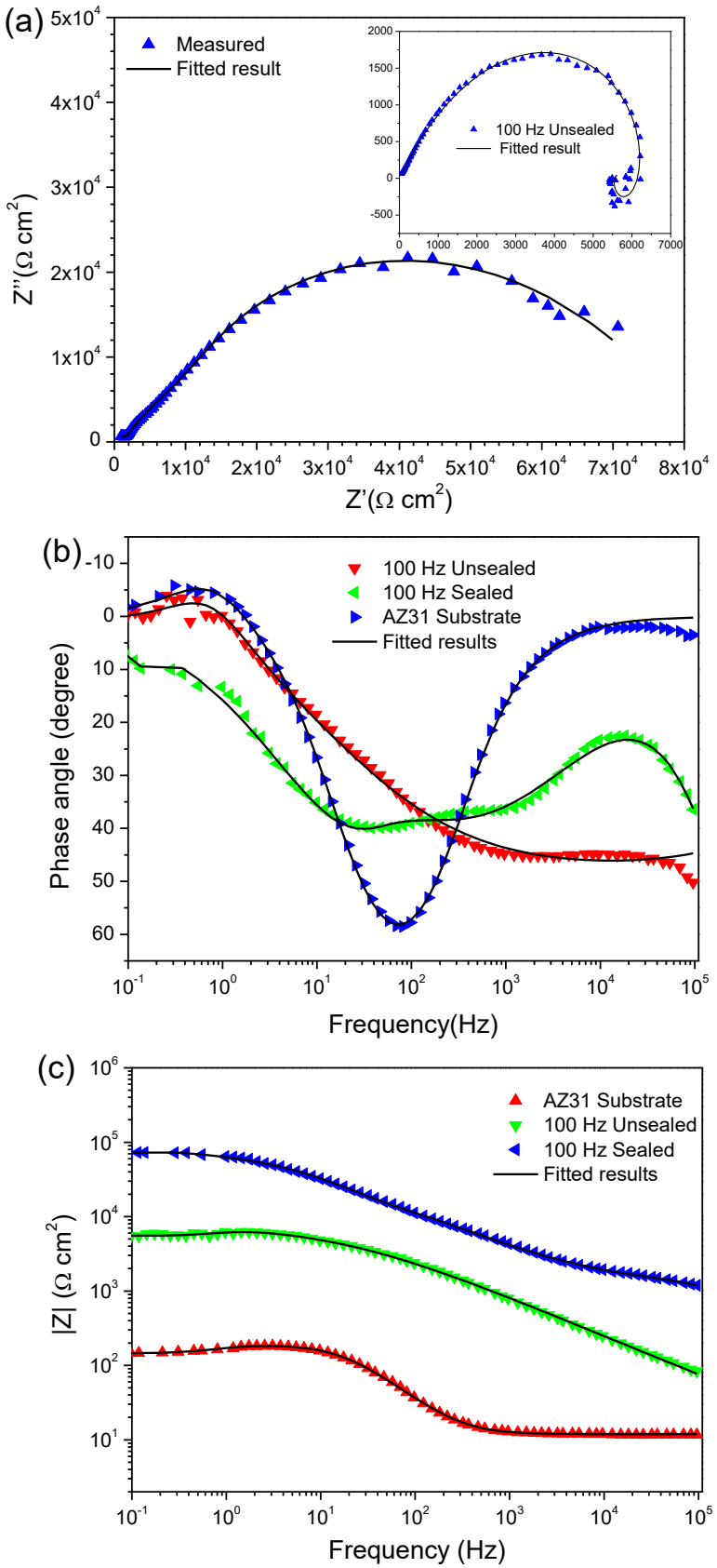

Figure 10. (a) Nyquist and (b),(c) Bode plots of bare alloy, unsealed and sealed PEO coatings formed for 600s in the aluminate-based electrolyte with addition 10 g l^{-1} $Na_2WO_4 \cdot 2H_2O$ under a current frequency of 100 Hz. Sequential lines correspond to fit using equivalent circuits of Fig. 12 and symbols correspond to experimental values.

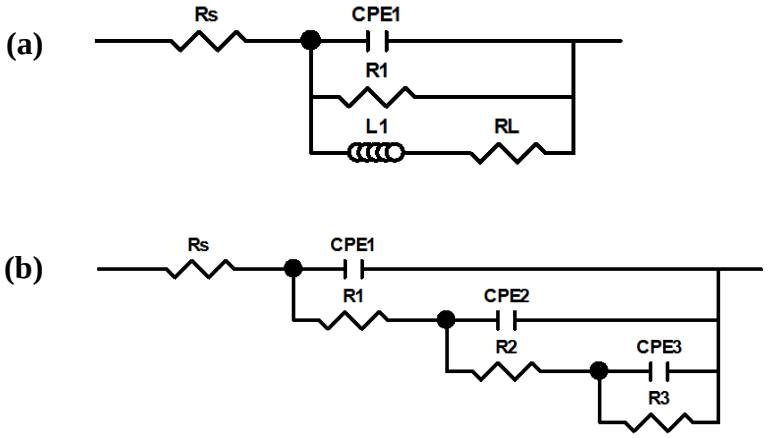

Figure 11. Equivalent circuits of the EIS plots for (a) uncoated and PEO coated but unsealed AZ31 Mg alloy and (b) sealed PEO coating in 3.5 wt.% NaCl solution.

Table 3. Fitting results of EIS plots of the uncoated and PEO coated AZ31 magnesium alloy under 100Hz after 1 h of immersion.

Samples	CPE1-T	CPE1-P	R_1 (Ωcm^2)	L(H)	R_L(Ωcm^2))
AZ31 Substrate	6.523×10^{-5}	0.8	175.9	135	55.62
PEO Coated Mg	1.047×10^{-5}	0.8	7704	5025	2165

Table 4. Fitting result of the EIS plot of the sealed PEO coating after 1 h of immersion.

R_S (Ωcm^2)	CPE-T ($\Omega^{-1}s^n cm^{-2}$)	CPE1-P	R1 ($k\Omega \cdot cm^2$)	CPE2-T ($\Omega^{-1}s^n cm^{-2}$)	CPE2-P	R2 ($k\Omega \cdot cm^2$)	CPE3-T ($\Omega^{-1}s^n cm^{-2}$)	CPE3-P	R3 ($k\Omega \cdot cm^2$)
26	7.056×10^{-8}	0.91	1.3	1.802×10^{-6}	0.8	37.42	1.785×10^{-7}	0.82	43.68

To evaluate the degradation behavior of the unsealed and sealed PEO coating, the values of total resistance ($R_{total}=R_1+R_2+R_3+R_L$) were calculated, it's 9869$\Omega \cdot cm^2$ for unsealed sample, and 82.4 $k\Omega \cdot cm^2$ for sealed coating. The distinction of R_{total} demonstrates that the sealed coating can slow down the corrosion rate of substrate better than unsealed coating.

The improvement of corrosion behavior can be partly attributed to the Ce-rich products

precipitated on the materials leading to a capacitive and resistive behavior of Ce-rich coating [49]. From the perspective of Ce conversion, after an immersion for duration of 1 h, the newly formed corrosion products containing Ce can act as a temporary protective layer together with the original PEO coating. Mohedano [22] pointed out that when corrosive media penetrates into the PEO coating, the number of Ce^{3+} ions in the sealed coating increases as a result of conversion by Ce-containing products, thus, the inner layer of the coating might be stabilized, which contributes to improvement of anticorrosion ability of the coating. From another point of view, sealing treatment of $Al(H_2PO_4)_3$ also contributed a lot to the protective property of the coating. Kamień [50] investigated the influence of aluminium phosphate on the properties of concrete. They noted that adding aluminium phosphate could reduce the permeability and improve the water tightness of concrete. This situation was attributed to the inactive phases formed between the phosphate ions and magnesium ions, which reduced the number of micro-pores in the concrete and increased the density of concrete. Recently, Feng [24] used aluminium tripolyphosphate to slow down corrosion rate of carbon steel, they found that ATP reacted with magnesium and calcium ions, a protective layer was formed on the carbon steel, the corrosion of carbon steel was effectively inhibited. As for the present case, when heated to around 250℃, the nature of the P-O-P bond of the original $Al(H_2PO_4)_3$ began to change from a linear structure to a small (three-or four-member) metaphosphate $Al(PO_4)_3$ ring structure [51]. The bonds of –P=O and –P-OH within the ring structure make it liable to chelate with various metal cations, forming a passive file and thus providing good corrosion protection. In the present case, the Mg^{2+} cations in the PEO coating might have chelated with ATP, increasing the cross-link density among phosphate chains within the ring structure to result in a better corrosive durability.

4. CONCLUSION

W-containing PEO coatings were fabricated in aluminate-based electrolyte with the addition of $Na_2WO_4{\cdot}2H_2O$. Adding $Na_2WO_4{\cdot}2H_2O$ to electrolyte not only accelerated the growth rate of the coating but also increased the thickness and surface roughness of the PEO coating. WO_3 and $W_{18}O_{49}$ were detected in the unsealed coating through XRD, $AlPO_4$, $AlH_2P_3O_{10}$ and $Al(HPO_4)_3$ were found in the two-step approach sealed coating, no Ce-containing oxide was detected by XRD. In addition, the addition of $Na_2WO_4{\cdot}2H_2O$ to the electrolyte was found to have improved the corrosion resistance of PEO coating, coating formed in aluminate electrolyte with 10 g l^{-1} $Na_2WO_4{\cdot}2H_2O$ manifested the best corrosion resistance. Corrosion mechanism of coatings changed after sealing treatment, dynamic polarization tests and EIS measurements indicated that the corrosion resistance of the PEO coatings had improved a lot by immersing in 3.5 wt.% NaCl solution for 1 h after being sealed by Ce-based solution and $Al(H_2PO_4)_3$ solution.

ACKNOWLEDGEMENT
The authors thank the National Natural Science Foundation of China (Grant Numbers: 51671084 and 51071066) for support of this work.

References

1. G. Barati Darband, M. Aliofkhazraei, P. Hamghalam and N. Valizade, *J. Magn. Alloy.*, 5 (2017) 74.

2. B. J .Han, D. D. Gu, Y. Yang, L. Fang, G. H. Peng and C. B. Yang, *Int. J. Electrochem. Sci.*, 12 (2017) 374.
3. J. Liang, P. Bala Srinivasan, C. Blawert and W. Dietzel, *Electrochim. Acta*, 55 (2010) 6802.
4. C.-E. Barchiche, E. Rocca, C. Juers, J. Hazan and J. Steinmetz, *Electrochim. Acta*, 53 (2007) 417.
5. L. Yu, J. H. Cao and Y. L. Cheng, *Surf. Coat. Technol.*, 276 (2015) 266.
6. F. F. Wei, W. Zhang, T. Zhang and F.H. Wang, *Int. J. Electrochem. Sci.*, 12 (2017) 155.
7. Y. L. Cheng, Z. M. Peng, X. Q. Wu, J. H. Cao, P. Skeldon and G.E. Thompson, *Electrochim. Acta.* 165 (2015) 301.
8. Y. Si, Z. Xiong, X. Zheng, M. Li and Q. Yang, *Int. J. Electrochem. Sci.*, 11 (2016) 3261.
9. H. N. Vatan, R. E. Kahrizsangi and M. K. Asgarani, *Int. J. Electrochem. Sci.*, 11 (2016) 929.
10. D. G. Barton, S. L. Soled and E. Iglesia, *Top. Catal.* 6 (1998) 87.
11. C. C. Tseng, J. L. Lee, T. H. Kuo, S. N. Kuo and K. H. Tseng, *Surf. Coat. Technol.*, 206 (2012) 3437.
12. Z. J. Li, Y. Yuan, P. P. Sun and X. Y. Jing, *ACS Appl. Mat. Interfaces.* 3 (2011) 3682.
13. H. Y. Zheng, Y. K. Wang, B. S. Li and G. R. Han, *Mater. Lett.*, 59 (2005) 139.
14. W. B. Tu, Y. L. Cheng, X. Y. Wang, T. Y. Zhan, J. X. Han and Y. L. Cheng, *J. Alloys Compd.*, 725 (2017) 199.
15. A. Melhem, G. Henrion, T. Czerwiec, J. L. Briancon, T. Duchanoy, F. Brochard and T. Belmonte, *Surf. Coat. Technol.* 205 (2011) 133.
16. J. A. Curran and T. W. Clyne, *Surf. Coat. Technol.* 199 (2005) 177.
17. U. Malayoglu, K. C. Tekin and S. Shrestha, *Surf. Coat. Technol.*, 205 (2010) 1793.
18. Z. J. Li, X. Y. Jing, Y. Yuan and M. L. Zhang, *Corros. Sci.*, 63 (2012) 358.
19. R. G. Hu, S. Zhang, J. F. Bu, C. J. Lin and G. L. Song, *Prog. Org. Coat.*, 73 (2012) 129.
20. B. Priet, G. Odemer, C. Blanc, K. Giffard and L. Arurault, *Surf. Coat. Technol.*, 307 (2016) 206.
21. M. Laleh, F. Kargar and A. S. Rouhaghdam, *J. Rare Earths*, 30 (2012) 1293.
22. M. Mohedano, C. Blawert and M. L. Zheludkevich, *Surf. Coat. Technol.*, 269 (2015) 145.
23. T. S. Lim, H. S. Ryu and S. H. Hong, *J. Electrochem. Soc.*, 160 (2013) 77.
24. X. G. Feng, R. L. Shi, X. Y. Lu, Y. W. Xu, X. F. Huang and D. Chen, *Corros. Sci.*, 124 (2017) 150.
25. R. Naderi and M. M. Attar, *Prog. Org. Coat.*, 66 (2009) 314.
26. R. Naderi and M. M. Attar, *Corros. Sci.*, 52 (2010) 1291.
27. Q. H. Lu and Y. H. Hu, *Trans. Nonferrous Metal. Soc. China*, 22 (2012) 483.
28. M. Vippola, S. Ahmaniemi, J. Keränen, P. Vuoristo, T. Lepistö, T. Mäntylä and E. Olsson, *Mater. Sci. Eng.*, A, 323 (2002) 1.
29. N. V. Phuong, B. R. Fazal and S. Moon, *Surf. Coat. Technol.*, 309 (2017) 86.
30. L. He, D. Chen and S. Shang, *J. Mater. Sci.*, 39 (2004) 4887.
31. R. O. Hussein, X. Nie and D. O. Northwood, *Electrochim. Acta*, 112 (2013) 111.
32. R. O. Hussein, P. Zhang, X. Nie, Y. Xia and D. O. Northwood, *Surf. Coat. Technol.*, 206 (2011) 1990.
33. R. Arrabal, A. Pardo, M. C. Merino, M. Mohedano, P. Casajús, E. Matykina, P. Skeldon and G. E. Thompson, *Corros. Sci.*, 52 (2010) 3738.
34. J. Liang, P. B. Srinivasan, C. Blawert, M. Störmer and W. Dietzel, *Electrochim. Acta*, 54 (2009) 3842.
35. A. H. Reshak, S. A. Khan and Z. A. Alahmed, *Opt. Mater.*, 37 (2014) 322.
36. S. F. Lu, B. S. Lou, Y. C. Yang, P. S. Wu, R. J. Chung and J. W. Lee, *Thin Solid Films*, 596 (2015) 87.
37. M. Sandhyarani, T. Prasadrao and N. Rameshbabu, *Appl. Surf. Sci.*, 317 (2014) 198.
38. Y. L. Cheng, T. Wang, S. X. Li, Y. L. Cheng, J. H. Cao and H. J. Xie, *Electrochim. Acta.* 225 (2017) 47.
39. H. P. Duan, C. W. Yan and F. H. Wang, *Electrochim. Acta*, 52 (2007) 3785.
40. Y. Shang, L. Wang, Z. Liu, D. Niu, Y. Wang and C. Liu, *Int. J. Electrochem. Sci.*, 11 (2016) 5234.

41. H. Tang, T. Wu, F. Xu, W. Tao and X. Jian, *Int. J. Electrochem. Sci.*, 12 (2017) 1377.
42. J. Hu, X. H. Zhao, S. W. Tang and M. R. Sun, *Surf. Coat. Technol.*, 201 (2006) 3814.
43. C. N. Cao, J. Q. Zhang, An Introduction to Electrochemical Impedance Spectroscopy, Science Press, Beijing (2002), China.
44. Z. Zhang, J. Q. Zhang, J. M. Wang and C. N. Cao, *Trans. Nonferrous Met. Soc. China*, 11 (2001) 284.
45. R. O. Hussein, D. O. Northwood and X. Nie, *Surf. Coat. Technol.*, 237 (2013) 357.
46. G. Song, A. Atrens, D. S. John, X. Wu and J. Nairn, *Corros. Sci.*, 39 (1997) 1981.
47. S. Gowtham, T. Arunnellaiappan and N. Rameshbabu, *Surf. Coat. Technol.*, 301 (2016) 63.
48. J. Zhao, K. Ouyang, X. Xie and J. Zhang, *Int. J. Electrochem. Sci.*, 12 (2017) 2400.
49. G. H. Wu, C. Y. Wang, Q. Zhang and P. C. Kang, *J. Alloys Compd.*, 461 (2008) 389.
50. L. M. Kamień, A. R. Kmita and Ł. Wójcik, *Ceram. Int.*, 40 (2014) 15663.
51. H. J. Han and D. P. Kim, *J. Sol-Gel Sci. Technol.*, 26 (2003) 223.